Journal of Magnetic Resonance **139,** 258–272 (1999)
Article ID jmre.1999.1766, available online at http://www.idealibrary.com on IDEAL®

Permeability Coefficients from NMR *q*-Space Data: Models with Unevenly Spaced Semi-permeable Parallel Membranes

Philip W. Kuchel[1] and Christopher J. Durrant*

*Department of Biochemistry and *School of Mathematics and Statistics, University of Sydney, NSW 2006, Australia*

Received November 2, 1998; revised March 18, 1999

The NMR "*q*-space" experiment conducted on water provides information on the sizes of repeated structures on the micrometer-length scale in heterogeneous samples, including cell suspensions or tissues. Under some circumstances these plots display coherence peaks, and it has been implied theoretically that the position of the peaks will vary with the rate of molecular exchange across the membranes. This has been demonstrated (qualitatively) with human erythrocytes in suspension. Thus, in the quest for a quantitative approach to the interpretation of such data, we address here the "inverse problem," namely the estimate of the permeability coefficient of membranes from *q*-space experiments. The present work describes theoretical predictions of *q*-space plots from molecules diffusing in a simple system of parallel semi-permeable membranes arranged with separations that alternate between two different values; this was designed to (loosely) mimic the intra- and extracellular compartments in a suspension of cells or a tissue. The development of the theory was facilitated by symbolic computation, and the analysis of synthetic data was shown to be achievable by the use of a three-layer back-propagation artificial neural network.

Key Words: **NMR; *q*-space; restricted diffusion; parallel planes; membrane permeability; neural networks.**

INTRODUCTION

The graph of NMR signal intensity in a pulsed field gradient spin-echo (PFGSE) experiment versus the scaled intensity of the magnetic field gradient pulses constitutes a "*q*-space plot" [(*1–5*); $q = (2\pi)^{-1}\ \gamma\delta g$ (units, m^{-1}), where γ is the nuclear magnetogyric ratio, δ is the duration of each of the two field gradient pulses, and g is the magnitude of the field gradient pulses]. This experiment has been used to record the translational diffusion behavior of solvents and solutes in heterogeneous systems, including yeast cells, human erythrocytes, and tissues (*1, 6, 7*). With some samples, *q*-space plots display "coherence" peaks whose maxima and minima occur at *q*-values that bear a simple mathematical relationship with the separation between the barriers (membranes) that restrict the molecular diffusion (*5, 8–13*). Thus, coherence effects have been demonstrated for isopentane diffusing in 100-μm capillaries that lie across the main field, $\mathbf{B}_0$, of the NMR magnet (*8*), heptane between glass microscope cover slips (*13*), and the first natural (and cellular) system, suspensions of human erythrocytes (*6*).

An analysis of the dependence of the PFGSE signal intensity on g for spins diffusing between evenly spaced parallel planes has been presented by Tanner (*14*). More recently, the solution for spins diffusing between impermeable parallel planes has been addressed in the context of *q*-space plots and diffusion–diffraction (*9, 15*).

In the present work spatially periodic two- and four-region systems, as depicted in Fig. 1, were considered. We derived expressions that describe the dependence of the PFGSE NMR signal intensity on the spatial separation between the barriers, the diffusion coefficients of the molecules that carry the spins, and the rate constant (permeability) that characterizes the exchange across the barriers between the regions.

The "inverse problem" that is addressed by an experimentalist, in the present context, is a complicated one. It is the attempt to determine the values of the intrinsic diffusion coefficients of the diffusing species in the various compartments of the sample, the physical dimensions of the spaces that restrict the diffusion, and the rate constants or permeabilities that characterize the exchange between the compartments. Traditionally this problem would be expected to be solved by regressing a mathematical function (that explicitly involves the various parameters) onto the experimental data. As will be seen below, the theory for even the relatively simple system considered here entails a "formula" that describes the NMR signal intensity as a function of q, but it is exceptionally complicated. However, the function is rapidly evaluated on a modern computer so it is a realistic proposition to simulate the behavior of the putative diffusion system.

Therefore, the experimental data analysis entails training an artificial neural network (ANN) with "synthetic" data that are the result of evaluating the analytical expression for a range of parameter values that are presumed to encompass those that occur naturally in the system under study. The "real" experimental data are then entered into the trained neural network that then yields as its output the set of parameter estimates. This approach to analyzing PFGSE data has been shown to be viable for data from molecules diffusing in real homogeneous, and simulated heterogeneous, systems (*16, 17*). Hence, the method was demonstrated in the present work as being theoretically viable for the systems under consideration.

[1] To whom correspondence should be addressed. E-mail: p.kuchel@biochem.usyd.edu.au.

1090-7807/99 $30.00

GENERAL THEORY

Master integral. The aim of the analysis is to derive the mathematical expression that describes the dependence of the PFGSE signal intensity on the experimental NMR parameters and the physical parameters that describe the sample. The expression for the spin-echo signal is obtained from the following integral that is evaluated over a "characteristic" spatial dimension of the sample (*5, 18*):

$$E[q, \Delta] = \int\int P[z_0]P[z_0|z; \Delta]\exp[i2\pi q(z - z_0)]dzdz_0, \quad [1]$$

where $E[q, \Delta]$ denotes the signal intensity in the PFGSE experiment acquired with Δ being the time between the magnetic field gradient pulses of duration δ, and $\delta \ll \Delta$. The latter implies the short gradient pulse approximation that is the basis of the simple form of the integral (e.g., *5, 18*); this integral contrasts with the more complicated one used for relatively large δ values or even a constant field gradient (e.g., *19*). The exponential term with its imaginary exponent already implies a solution that is periodic in qz.

$P[z_0]dz_0$ is the probability of a spin being located at z_0 at the start of the diffusion-measurement period, and $P[z_0|z; \Delta]$ is as the conditional probability density. The normalized initial spin-density $P[z_0]$ is simply the probability density of any given coordinate on the specified interval; if the interval is $[0, (a + b)/2]$, the probability density is $2/(a + b)$.

Master diffusion equation. The main mathematical task is to determine the expression for P. In overview, the problem entails solving the self-diffusion equation, expressed in terms of the conditional probability density (e.g., *14, 15, 19–21*). In the present context P is a function of only time, t, and one spatial Cartesian coordinate, z, that is in the direction of the magnetic field gradient pulses used in the PFGSE experiment. Thus,

$$D\frac{\partial^2 P}{\partial z^2} = \frac{\partial P}{\partial t}. \quad [2]$$

P is a Green's function and its use in solving the present class of problem is described more fully elsewhere (e.g., *19, 22*).

In more detail, Eq. [1] can be solved by using "separation of variables," which entails assuming that P can be separated into the product of two functions that depend exclusively on the spatial coordinate (in this case z and z_0), and t (e.g., *19*). Thus the solution of the time-dependent equation is

$$T[t] = \exp[-\omega^2 t], \quad [3]$$

where ω is the so-called separation constant (or eigenvalue). Since P decreases with time, ω is specified as being positive-real. The general solution of the spatial equation is

$$Z[z] = A\cos\left[\frac{\omega z}{\sqrt{D}}\right] + B\sin\left[\frac{\omega z}{\sqrt{D}}\right]. \quad [4]$$

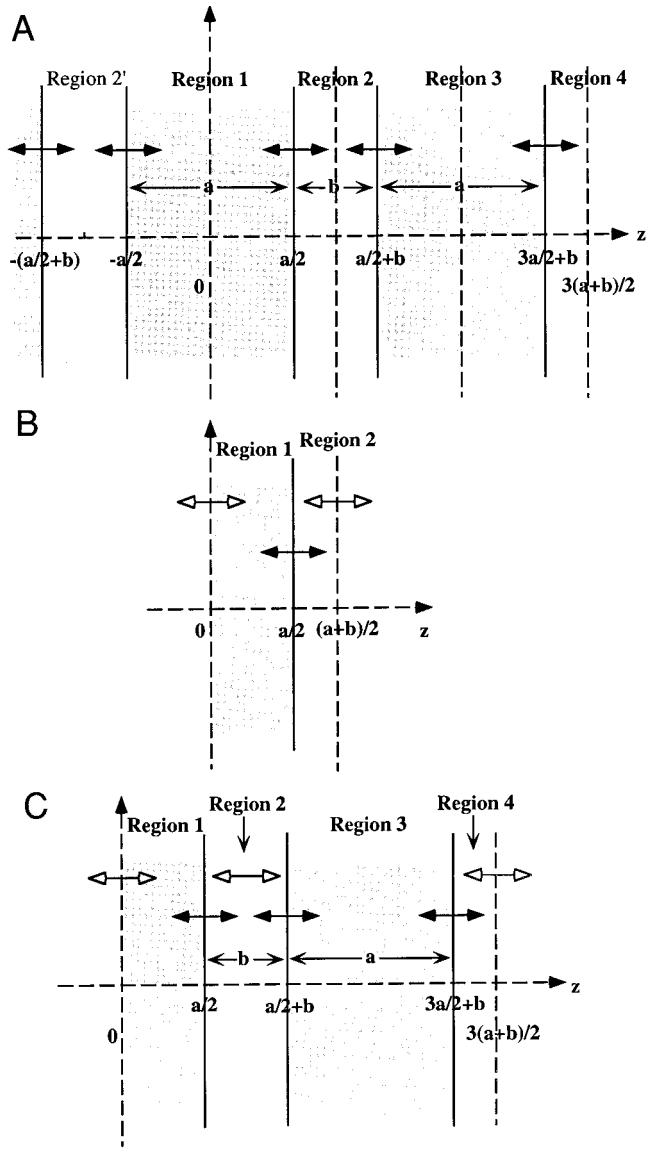

FIG. 1. System of periodically arranged parallel planes, with diffusion within each region and across the "membranes" (barriers) between them. The membranes are separated by the alternating distances a and b. The possibility of diffusive exchange between the regions is indicated by the solid double-headed arrows. The origin of the Cartesian coordinate system is at $z = 0$, the interface between the central regions lies at $z = a/2$, and the midplane of Region 2 lies at $z = (a + b)/2$, etc. (A) The shaded regions can be interpreted as being separated by parallel planes perpendicular to the page and, in the case of a suspension of cells (e.g., erythrocytes (*6, 12*)), these planes correspond to the cell membranes. Regions 2 and 2′, etc., correspond to the extracellular space in a cell suspension. B is the canonical two-region unit that was used in the boundary value problem discussed in the text. The vertical dotted lines denote planes of symmetry in the regions and the solid lines denote the permeable plane (membrane) between them. The open double-headed arrows indicate the free movement of spins across the imaginary planes of symmetry in each region (boundary value equations, Eqs. [7a] and [7b]). C is the canonical four-region unit used in the analysis that is described in the text.

The overall solution is the product of Eqs. [3] and [4], summed over a series of values of the separation constant. In analyzing the two-region system shown in Fig. 1B, we

define $Z_1 \equiv P_1 + Q_1$, $Z_2 \equiv P_2 + Q_2$; and for the four-region system in Fig. 1C we define $Z_3 \equiv P_3 + Q_3$, and $Z_4 \equiv P_4 + Q_4$ where the P and Q functions are referred to as *symmetric* and *antisymmetric* series solutions. This notation is used because when the boundary equations (Eqs. [7] and [8] below) are applied to the general solution the leading term of one series is simply a cosine function (an even function) and for the other boundary conditions the leading term is a sine function (an odd function). Thus the general solution is given by the sum of the series

$$P_i[z] = \sum_{n=1}^{\infty} \left(A_{i,n}\cos\left[\frac{\omega_n z}{\sqrt{D_i}}\right] + B_{i,n}\sin\left[\frac{\omega_n z}{\sqrt{D_i}}\right]\right)\exp[-\omega_n^2 t], \quad i = 1, 2 \text{ or } 1, \ldots, 4, \quad [5]$$

where the system involves the diffusion coefficients, D_i, (units, $m^2\ s^{-1}$) such that $D_3 = D_1$ and $D_4 = D_2$. The formal expression for the antisymmetric solution is the same as for Eq. [5] but the different boundary value equations dictate that the separation constants (ζ_i; eigenvalues) are different, as are the coefficients in the series. Thus,

$$Q_i[z] = \sum_{n=1}^{\infty} \left(C_{i,n}\cos\left[\frac{\zeta_n z}{\sqrt{D_i}}\right] + D_{i,n}\sin\left[\frac{\zeta_n z}{\sqrt{D_i}}\right]\right)\exp[-\zeta_n^2 t], \quad i = 1, 2 \text{ or } 1, \ldots, 4. \quad [6]$$

THEORY: PERIODIC FOUR-REGION SYSTEM

The system of parallel planes depicted in Fig. 1 can be considered either as repeating units of two or four regions. Since the two-region system is a subcase of the four-region one only the latter is analyzed in detail here. The next step is to derive the boundary condition equations; these are similar to those used previously (*14, 15*) but note that this earlier work did not consider unevenly spaced planes or, in the second reference, permeable planes.

Boundary condition equations. These are

$$\left.\frac{dP_1}{dz}\right|_{z=l_1} = 0, \quad [7a]$$

$$\left.\frac{dP_4}{dz}\right|_{z=l_7} = 0, \quad [7b]$$

$$D_i\left.\frac{dP_i}{dz}\right|_{z=l_{2i}} = D_{i+1}\left.\frac{dP_{i+1}}{dz}\right|_{z=l_{2i}}, \quad i = 1, \ldots, 3, \quad [7c]$$

$$D_i\left.\frac{dP_i}{dz}\right|_{z=l_{2i}} = M(P_{i+1} - P_i)\Big|_{z=l_{2i}}, \quad i = 1, \ldots, 3, \quad [7d]$$

where $l_1 = 0$, $l_2 = a/2$, $l_3 = (a + b)/2$, $l_4 = a/2 + b$, $l_5 = a + b$, $l_6 = 3a/2 + b$, and $l_7 = 3(a + b)$. The first two of these equations specify the fact that spins do not pass out of the "outer" regions. Equation [7c] indicates that the fluxes of spins between Regions 1 and 2, Regions 2 and 3, and Regions 3 and 4 are each equal in either direction. Equation [7d] specifies the fact that the flux of spins across each interface (membrane) is proportional to the difference between P on either side of the membrane; the proportionality constant is the permeability coefficient M (units, $m\ s^{-1}$). The mass-transfer (or heat-transfer; *23*) analogue of this situation is readily visualized. There is also a counterpart to Eq. [7d] for P_4, but it is redundant in the analysis.

The boundary conditions for the antisymmetric solutions are different from the first two above (Eqs. [7a] and [7b]) but the same as the others (Eqs. [7c] and [7d]). Their physical interpretations are analogous to the previous cases:

$$Q_{1,4}|_{z=l_1,l_7} = 0, \quad [8a]$$

$$D_i\left.\frac{dQ_i}{dz}\right|_{z=l_{2i}} = D_{i+1}\left.\frac{dQ_{i+1}}{dz}\right|_{z=l_{2i}}, \quad i = 1, \ldots, 3, \quad [8b]$$

$$D_i\left.\frac{dQ_i}{dz}\right|_{z=l_{2i}} = M(Q_{i+1} - Q_i)\Big|_{z=l_{2i}}, \quad i = 1, \ldots, 3. \quad [8c]$$

The next step is to obtain the two boundary-condition transcendental equations that are solved to yield the roots (eigenvalues), ω_n and ζ_n, thus satisfying the boundary equations. These are usually derived by applying the process of "Gaussian elimination" to the two sets of homogeneous simultaneous linear algebraic equations in which the "variables" are taken to be the coefficients $A_{i,m}$ and $B_{i,m}$, and $C_{i,m}$ and $D_{i,m}$, respectively. This involves expressing in matrix form both sets of eight boundary equations, using the overall expressions for P (Eq. [7]) and Q (Eq. [8]), respectively. The derivation of the individual elements of the matrices are straightforward but tedious and the details, if required, can be requested from the corresponding author.

$$
\begin{bmatrix}
0 & 1 & 0 \\
0 & 0 & 0 \\
-\sqrt{D_1}\sin\left[\frac{\omega_n a}{\sqrt{D_1}2}\right] & 0 & \sqrt{D_2}\sin\left[\frac{\omega_n a}{\sqrt{D_2}2}\right] \\
0 & 0 & -\sqrt{D_2}\sin\left[\frac{\omega_n (a/2+b)}{\sqrt{D_2}}\right] \\
0 & 0 & 0 \\
\left(-\sin\left[\frac{\omega_n a}{\sqrt{D_1}2}\right]\omega_n\sqrt{D_1} + M\cos\left[\frac{\omega_n a}{\sqrt{D_1}2}\right]\right) & 0 & -M\cos\left[\frac{\omega_n a}{\sqrt{D_2}2}\right] \\
0 & 0 & \left(-\sin\left[\frac{\omega_n (a/2+b)}{\sqrt{D_2}}\right]\omega_n\sqrt{D_2} + M\cos\left[\frac{\omega_n (a/2+b)}{\sqrt{D_2}}\right]\right) \\
0 & 0 & 0
\end{bmatrix}
\cdots
$$

$$
\begin{bmatrix}
0 & 0 \\
0 & 0 \\
-\sqrt{D_2}\cos\left[\frac{\omega_n a}{\sqrt{D_2}2}\right] & 0 \\
\sqrt{D_2}\cos\left[\frac{\omega_n (a/2+b)}{\sqrt{D_2}}\right] & \sqrt{D_1}\sin\left[\frac{\omega_n (a/2+b)}{\sqrt{D_1}}\right] \\
0 & -\sqrt{D_1}\sin\left[\frac{\omega_n (3a/2+b)}{\sqrt{D_1}}\right] \\
-M\sin\left[\frac{\omega_n a}{\sqrt{D_2}2}\right] & 0 \\
\left(\cos\left[\frac{\omega_n (a/2+b)}{\sqrt{D_2}}\right]\omega_n\sqrt{D_2} + M\sin\left[\frac{\omega_n (a/2+b)}{\sqrt{D_2}}\right]\right) & -M\cos\left[\frac{\omega_n (a/2+b)}{\sqrt{D_1}}\right] \\
0 & \left(-\sin\left[\frac{\omega_n (3a/2+b)}{\sqrt{D_1}}\right]\omega_n\sqrt{D_1} + M\cos\left[\frac{\omega_n (3a/2+b)}{\sqrt{D_1}}\right]\right)
\end{bmatrix}
\cdots
$$

$$
\begin{bmatrix}
0 & 0 & 0 \\
0 & -\sin\left[\frac{\omega_n 3(a+b)}{\sqrt{D_2}2}\right] & \cos\left[\frac{\omega_n 3(a+b)}{\sqrt{D_2}2}\right] \\
0 & 0 & 0 \\
-\sqrt{D_1}\cos\left[\frac{\omega_n (a/2+b)}{\sqrt{D_1}}\right] & 0 & 0 \\
\sqrt{D_1}\cos\left[\frac{\omega_n (3a/2+b)}{\sqrt{D_1}}\right] & \sqrt{D_2}\sin\left[\frac{\omega_n (3a/2+b)}{\sqrt{D_2}}\right] & -\sqrt{D_2}\cos\left[\frac{\omega_n (3a/2+b)}{\sqrt{D_2}}\right] \\
0 & 0 & 0 \\
-M\sin\left[\frac{\omega_n (a/2+b)}{\sqrt{D_1}}\right] & 0 & 0 \\
\left(\cos\left[\frac{\omega_n (3a/2+b)}{\sqrt{D_1}}\right]\omega_n\sqrt{D_1} + M\sin\left[\frac{\omega_n (3a/2+b)}{\sqrt{D_1}}\right]\right) & -M\cos\left[\frac{\omega_n (3a/2+b)}{\sqrt{D_2}}\right] & -M\sin\left[\frac{\omega_n (3a/2+b)}{\sqrt{D_2}}\right]
\end{bmatrix}
$$

$$
\times
\begin{bmatrix}
A_{1,n} \\ B_{1,n} \\ A_{2,n} \\ B_{2,n} \\ A_{3,n} \\ B_{3,n} \\ A_{4,n} \\ B_{4,n}
\end{bmatrix}
=
\begin{bmatrix}
0 \\ 0 \\ 0 \\ 0 \\ 0 \\ 0 \\ 0 \\ 0
\end{bmatrix},
\quad [9]
$$

and

$$
\begin{bmatrix}
1 & 0 & 0 \\
0 & 0 & 0 \\
0 & \sqrt{D_1}\cos\left[\dfrac{\zeta_n a}{\sqrt{D_1}2}\right] & \sqrt{D_2}\sin\left[\dfrac{\zeta_n a}{\sqrt{D_2}2}\right] \\
0 & 0 & -\sqrt{D_2}\sin\left[\dfrac{\zeta_n(a/2+b)}{\sqrt{D_2}}\right] \\
0 & 0 & 0 \\
\left(-\sin\left[\dfrac{\zeta_n a}{\sqrt{D_1}2}\right]\zeta_n\sqrt{D_1}+M\cos\left[\dfrac{\zeta_n a}{\sqrt{D_1}2}\right]\right) & 0 & -M\cos\left[\dfrac{\zeta_n a}{\sqrt{D_2}2}\right] \\
0 & 0 & \left(-\sin\left[\dfrac{\zeta_n(a/2+b)}{\sqrt{D_2}}\right]\zeta_n\sqrt{D_2}+M\cos\left[\dfrac{\zeta_n(a/2+b)}{\sqrt{D_2}}\right]\right) \\
0 & 0 & 0
\end{bmatrix}
\cdots
$$

$$
\begin{bmatrix}
0 & 0 \\
0 & 0 \\
-\sqrt{D_2}\cos\left[\dfrac{\zeta_n a}{\sqrt{D_2}2}\right] & 0 \\
\sqrt{D_2}\cos\left[\dfrac{\zeta_n(a/2+b)}{\sqrt{D_2}}\right] & \sqrt{D_1}\sin\left[\dfrac{\zeta_n(a/2+b)}{\sqrt{D_1}}\right] \\
0 & -\sqrt{D_1}\sin\left[\dfrac{\zeta_n(3a/2+b)}{\sqrt{D_1}}\right] \\
-M\sin\left[\dfrac{\zeta_n a}{\sqrt{D_2}2}\right] & 0 \\
\left(\cos\left[\dfrac{\zeta_n(a/2+b)}{\sqrt{D_2}}\right]\zeta_n\sqrt{D_2}+M\sin\left[\dfrac{\zeta_n(a/2+b)}{\sqrt{D_2}}\right]\right) & -M\cos\left[\dfrac{\zeta_n(a/2+b)}{\sqrt{D_1}}\right] \\
0 & \left(-\sin\left[\dfrac{\zeta_n(3a/2+b)}{\sqrt{D_1}}\right]\zeta_n\sqrt{D_1}+M\cos\left[\dfrac{\zeta_n(3a/2+b)}{\sqrt{D_1}}\right]\right)
\end{bmatrix}
\cdots
$$

$$
\begin{bmatrix}
0 & 0 & 0 \\
0 & \cos\left[\dfrac{\zeta_n 3(a+b)}{\sqrt{D_2}2}\right] & \sin\left[\dfrac{\zeta_n 3(a+b)}{\sqrt{D_2}2}\right] \\
0 & 0 & 0 \\
-\sqrt{D_1}\cos\left[\dfrac{\zeta_n(a/2+b)}{\sqrt{D_1}}\right] & 0 & 0 \\
\sqrt{D_1}\cos\left[\dfrac{\zeta_n(3a/2+b)}{\sqrt{D_1}}\right] & \sqrt{D_2}\sin\left[\dfrac{\zeta_n(3a/2+b)}{\sqrt{D_2}}\right] & -\sqrt{D_2}\cos\left[\dfrac{\zeta_n(3a/2+b)}{\sqrt{D_2}}\right] \\
0 & 0 & 0 \\
-M\sin\left[\dfrac{\zeta_n(a/2+b)}{\sqrt{D_1}}\right] & 0 & 0 \\
\left(\cos\left[\dfrac{\zeta_n(3a/2+b)}{\sqrt{D_1}}\right]\zeta_n\sqrt{D_1}+M\sin\left[\dfrac{\zeta_n(3a/2+b)}{\sqrt{D_1}}\right]\right) & -M\cos\left[\dfrac{\zeta_n(3a/2+b)}{\sqrt{D_2}}\right] & -M\sin\left[\dfrac{\zeta_n(3a/2+b)}{\sqrt{D_2}}\right]
\end{bmatrix}
\times
\begin{bmatrix}
C_{1,n} \\ D_{1,n} \\ C_{2,n} \\ D_{2,n} \\ C_{3,n} \\ D_{3,n} \\ C_{4,n} \\ D_{4,n}
\end{bmatrix}
=
\begin{bmatrix}
0 \\ 0 \\ 0 \\ 0 \\ 0 \\ 0 \\ 0 \\ 0
\end{bmatrix}. \quad [10]
$$

Roots of the two boundary condition transcendental equations. For Eqs. [9] and [10] to have nontrivial solutions the determinant of their respective matrices must be zero. The expressions for these determinants cannot be easily derived "by hand" but they are readily (and rapidly) derived by symbolic computation; in *Mathematica* (*24*), the Det function generates the analytical expressions. In practice the determinants were left unexpressed and were evaluated numerically for specified values of, a, b, D_1, D_2, and M. The determination of the roots was readily achieved by using the FindRoot function operating on each determinant.

The coefficients of the symmetric and antisymmetric spatial equations. A reduced form of Eq. [9] was used to obtain the expressions for $A_{i,n}$ and $B_{i,n}$ in terms of $A_{1,n}$, and similarly for $C_{i,n}$ and $D_{i,n}$ in terms of $D_{1,n}$ from Eq. [10]. The numerical values of these coefficients were obtained by substituting the relevant values of ω_n or ζ_n into the expressions and using Cramer's rule on the determinant of the matrix to yield the values of $A_{i,n}$ and $B_{i,n}$, $i = 2, \ldots, 4$, and of $C_{i,n}$ and $D_{i,n}$, $i = 2, \ldots, 4$, respectively. The matrix forms of the equations are

$$
\begin{bmatrix}
0 & 0 \\
\sqrt{D_2}\sin\left[\frac{\omega_n a}{\sqrt{D_2}2}\right] & -\sqrt{D_2}\cos\left[\frac{\omega_n a}{\sqrt{D_2}2}\right] \\
-\sqrt{D_2}\sin\left[\frac{\omega_n(a/2+b)}{\sqrt{D_2}}\right] & \sqrt{D_2}\cos\left[\frac{\omega_n(a/2+b)}{\sqrt{D_2}}\right] \\
0 & 0 \\
\left(-\sin\left[\frac{\omega_n(a/2+b)}{\sqrt{D_2}2}\right]\omega_n\sqrt{D_2} + M\cos\left[\frac{\omega_n(a/2+b)}{\sqrt{D_2}2}\right]\right) & \left(\cos\left[\frac{\omega_n(a/2+b)}{\sqrt{D_2}2}\right]\omega_n\sqrt{D_2} + M\sin\left[\frac{\omega_n(a/2+b)}{\sqrt{D_2}2}\right]\right) \\
0 & 0 \\
0 & 0 \\
0 & 0 \\
\sqrt{D_1}\sin\left[\frac{\omega_n(a/2+b)}{\sqrt{D_1}}\right] & -\sqrt{D_1}\cos\left[\frac{\omega_n(a/2+b)}{\sqrt{D_1}}\right] \\
-\sqrt{D_1}\sin\left[\frac{\omega_n(3a/2+b)}{\sqrt{D_1}}\right] & \sqrt{D_1}\cos\left[\frac{\omega_n(3a/2+b)}{\sqrt{D_1}}\right] \\
-M\cos\left[\frac{\omega_n(a/2+b)}{\sqrt{D_1}2}\right] & -M\sin\left[\frac{\omega_n(a/2+b)}{\sqrt{D_1}2}\right] \\
\left(-\sin\left[\frac{\omega_n(3a/2+b)}{\sqrt{D_1}}\right]\omega_n\sqrt{D_1} + M\cos\left[\frac{\omega_n(3a/2+b)}{\sqrt{D_1}}\right]\right) & \left(\cos\left[\frac{\omega_n(3a/2+b)}{\sqrt{D_1}}\right]\omega_n\sqrt{D_1} + M\sin\left[\frac{\omega_n(3a/2+b)}{\sqrt{D_1}}\right]\right)
\end{bmatrix}
\ldots
$$

$$
\begin{bmatrix}
-\sin\left[\frac{\omega_n 3(a+b)}{\sqrt{D_2}2}\right] & \cos\left[\frac{\omega_n 3(a+b)}{\sqrt{D_2}2}\right] \\
0 & 0 \\
0 & 0 \\
\sqrt{D_2}\sin\left[\frac{\omega_n(3a/2+b)}{\sqrt{D_2}}\right] & -\sqrt{D_2}\cos\left[\frac{\omega_n(3a/2+b)}{\sqrt{D_2}}\right] \\
0 & 0 \\
-M\cos\left[\frac{\omega_n(3a/2+b)}{\sqrt{D_2}}\right] & -M\sin\left[\frac{\omega_n(3a/2+b)}{\sqrt{D_2}}\right]
\end{bmatrix}
\begin{bmatrix} A_{2,n} \\ B_{2,n} \\ A_{3,n} \\ B_{3,n} \\ A_{4,n} \\ B_{4,n} \end{bmatrix}
= A_{1,n}
\begin{bmatrix} 0 \\ \sqrt{D_1}\sin\left[\frac{\omega_n a}{\sqrt{D_1}2}\right] \\ 0 \\ 0 \\ 0 \\ 0 \end{bmatrix}, \quad [11a]
$$

and

$$\begin{bmatrix} 0 & 0 & \cdots \\ \sqrt{D_2}\sin\left[\frac{\zeta_n a}{\sqrt{D_2}2}\right] & -\sqrt{D_2}\cos\left[\frac{\zeta_n a}{\sqrt{D_2}2}\right] & \\ -\sqrt{D_2}\sin\left[\frac{\zeta_n(a/2+b)}{\sqrt{D_2}}\right] & \sqrt{D_2}\cos\left[\frac{\zeta_n(a/2+b)}{\sqrt{D_2}}\right] & \\ 0 & 0 & \\ \left(-\sin\left[\frac{\zeta_n(a/2+b)}{\sqrt{D_2}2}\right]\zeta_n\sqrt{D_2}+M\cos\left[\frac{\zeta_n(a/2+b)}{\sqrt{D_2}}\right]\right) & \left(\cos\left[\frac{\zeta_n(a/2+b)}{\sqrt{D_2}}\right]\zeta_n\sqrt{D_2}+M\sin\left[\frac{\zeta_n(a/2+b)}{\sqrt{D_2}}\right]\right) & \\ 0 & 0 & \end{bmatrix}$$

$$\begin{bmatrix} 0 & 0 & \cdots \\ 0 & 0 & \\ \sqrt{D_1}\sin\left[\frac{\zeta_n(a/2+b)}{\sqrt{D_1}}\right] & -\sqrt{D_1}\cos\left[\frac{\zeta_n(a/2+b)}{\sqrt{D_1}}\right] & \\ -\sqrt{D_1}\sin\left[\frac{\zeta_n(3a/2+b)}{\sqrt{D_1}}\right] & \sqrt{D_1}\cos\left[\frac{\zeta_n(3a/2+b)}{\sqrt{D_1}}\right] & \\ -M\cos\left[\frac{\omega\zeta_n(a/2+b)}{\sqrt{D_1}}\right] & -M\sin\left[\frac{\zeta_n(a/2+b)}{\sqrt{D_1}}\right] & \\ \left(-\sin\left[\frac{\zeta_n(3a/2+b)}{\sqrt{D_1}}\right]\zeta_n\sqrt{D_1}+M\cos\left[\frac{\zeta_n(3a/2+b)}{\sqrt{D_1}}\right]\right) & \left(\cos\left[\frac{\zeta_n(3a/2+b)}{\sqrt{D_1}}\right]\zeta_n\sqrt{D_1}+M\sin\left[\frac{\zeta_n(3a/2+b)}{\sqrt{D_1}}\right]\right) & \end{bmatrix}$$

$$\begin{bmatrix} \cos\left[\frac{\zeta_n 3(a+b)}{\sqrt{D_2}2}\right] & \sin\left[\frac{\zeta_n 3(a+b)}{\sqrt{D_2}2}\right] \\ 0 & 0 \\ 0 & 0 \\ \sqrt{D_2}\sin\left[\frac{\zeta_n(3a/2+b)}{\sqrt{D_2}}\right] & -\sqrt{D_2}\cos\left[\frac{\zeta_n(3a/2+b)}{\sqrt{D_2}}\right] \\ 0 & 0 \\ -M\cos\left[\frac{\zeta_n(3a/2+b)}{\sqrt{D_2}}\right] & -M\sin\left[\frac{\zeta_n(3a/2+b)}{\sqrt{D_2}}\right] \end{bmatrix} \begin{bmatrix} C_{2,n} \\ D_{2,n} \\ C_{3,n} \\ D_{3,n} \\ C_{4,n} \\ D_{4,n} \end{bmatrix} = D_{1,n} \begin{bmatrix} 0 \\ -\sqrt{D_1}\cos\left[\frac{\zeta_n a}{\sqrt{D_1}2}\right] \\ 0 \\ 0 \\ 0 \\ 0 \end{bmatrix}. \quad [11b]$$

Thus, from Eq. [11a]

$$P_1 = \sum_{n=1}^{\infty} A_{1,n}\cos\left[\frac{\omega_n z}{\sqrt{D_1}}\right]\exp[-\omega_n^2 t], \quad [12a]$$

and

$$P_i = \sum_{n=1}^{\infty} A_{i,n}F_i\exp[-\omega_n^2 t],\ i = 2, \ldots, 4, \quad [12b]$$

where

$$F_i \equiv F_i\left[\cos\left[\frac{\omega_n z}{\sqrt{D_i}}\right], \sin\left[\frac{\omega_n z}{\sqrt{D_i}}\right]\right],\ i = 2, \ldots, 4. \quad [12c]$$

Similarly, the antisymmetric series solution, expressed in terms of $D_{1,n}$, was obtained from Eq. [11b] by using Cramer's rule.

The initial condition and the coefficients of the spatial equations. The next task is to obtain the expressions for $A_{1,n}$ and $D_{1,n}$. First, the propagators for the four regions are added to give the overall propagator

$$P = G_1(P_1 + Q_1) + G_2(P_2 + Q_2) + G_3(P_3 + Q_3) + G_4(P_4 + Q_4), \quad [13a]$$

where

$$G_i \equiv G_i[z; l_i, l_{i+k}] = H[z - l_i]H[l_{i+k} - z] \quad [13b]$$

and

$$H[z - l_i] = \begin{cases} 0, & z < l_i \\ 1, & z > l_i \end{cases} \qquad [13c]$$

and

$$H[l_{i+k} - z] = \begin{cases} 1, & z < l_{i+k} \\ 0, & z > l_{i+k} \end{cases}, \qquad [13d]$$

and where i and k are dummy indices, and $k > i$.

In words, the unit step function has the value 1 when its argument is positive, and zero when it is negative. The step "feature" resides where the argument is zero.

Because the system of equations is a Sturm–Liouville one (e.g., *26, 27*), the above cosine and sine functions are orthogonal on the integration interval. Hence, the overall expression for P is

$$P = \sum_{n=1}^{\infty} \{A_{1,n}P^{(n)}[z]\exp[-\omega_n^2 t] + D_{1,n}Q^{(n)}[z]\exp[-\zeta_n^2 t]\}, \qquad [14a]$$

where we define the orthogonal functions as

$$P^{(n)} = P_1G_1[z; l_1, l_2] + P_2G_2[z; l_2, l_4] + P_3G_3[z; l_4, l_6] + P_4G_4[z; l_6, l_7] \qquad [14b]$$

and

$$Q^{(n)} = Q_1G_1[z; l_1, l_2] + Q_2G_2[z; l_2, l_4] + Q_3G_3[z; l_4, l_6] + Q_4G_4[z; l_6, l_7]. \qquad [14c]$$

Second, the initial condition is that of the planar delta-function source (*19, 28, 29*), thus,

$$\delta[z - z_0] = \sum_{n=1}^{\infty} \{A_{1,n}P^{(n)}[z] + D_{1,n}Q^{(n)}[z]\}. \qquad [15]$$

Equations [14b] and [14c] are combined and multiplied by $P^{(n)}[z] + Q^{(n)}[z]$ and then integrated over the whole interval $[0, 3(a + b)/2]$. This yields expressions for $A_{1,n}$ and $D_{1,n}$ because the integral on the right is nonzero only when $m = n$, and from the "sampling" property of the delta function (*25*), we obtain

$$\int_0^{3(a+b)/2} \delta[z - z_0]P^{(m)}[z]dz = A_{1,n}\int_0^{3(a+b)/2} (P^{(m)}[z])^2 dz, \qquad [16a]$$

and

$$\int_0^{3(a+b)/2} \delta[z - z_0]Q^{(m)}[z]dz = D_{1,n}\int_0^{3(a+b)/2} (Q^{(m)}[z])^2 dz. \qquad [16b]$$

Hence,

$$P^{(m)}[z_0] = A_{1,n}\int_0^{3(a+b)/2} (P^{(m)}[z])^2 dz, \qquad [16c]$$

and

$$Q^{(m)}[z_0] = D_{1,n}\int_0^{3(a+b)/2} (Q^{(m)}[z])^2 dz. \qquad [16d]$$

Thus, in expanded form, the expression for $A_{1,n}$ is

$$A_{1,n} = \frac{\left(G_1\cos\left[\frac{\omega_n z_0}{\sqrt{D_1}}\right] + G_2\left\{\left(\frac{\Xi_1}{\Xi}\right)\cos\left[\frac{\omega_n z_0}{\sqrt{D_2}}\right] + \left(\frac{\Xi_2}{\Xi}\right)\sin\left[\frac{\omega_n z_0}{\sqrt{D_2}}\right]\right\} + G_3\left\{\left(\frac{\Xi_3}{\Xi}\right)\cos\left[\frac{\omega_n z_0}{\sqrt{D_1}}\right] + \left(\frac{\Xi_4}{\Xi}\right)\sin\left[\frac{\omega_n z_0}{\sqrt{D_1}}\right]\right\} + G_4\left\{\left(\frac{\Xi_5}{\Xi}\right)\cos\left[\frac{\omega_n z_0}{\sqrt{D_2}}\right] + \left(\frac{\Xi_6}{\Xi}\right)\sin\left[\frac{\omega_n z_0}{\sqrt{D_2}}\right]\right\} \right)}{\left(\int_0^{a/2}\left(\cos\left[\frac{\omega_n z}{\sqrt{D_1}}\right]\right)^2 dz + \int_{a/2}^{a/2+b}\left(\left(\frac{\Xi_1}{\Xi}\right)\cos\left[\frac{\omega_n z}{\sqrt{D_2}}\right] + \left(\frac{\Xi_2}{\Xi}\right)\sin\left[\frac{\omega_n z}{\sqrt{D_2}}\right]\right)^2 dz + \int_{a/2+b}^{3a/2+b}\left(\left(\frac{\Xi_3}{\Xi}\right)\cos\left[\frac{\omega_n z}{\sqrt{D_1}}\right] + \left(\frac{\Xi_4}{\Xi}\right)\sin\left[\frac{\omega_n z}{\sqrt{D_1}}\right]\right)^2 dz + \int_{3a/2+b}^{3(a+b)/2}\left(\left(\frac{\Xi_5}{\Xi}\right)\cos\left[\frac{\omega_n z}{\sqrt{D_2}}\right] + \left(\frac{\Xi_6}{\Xi}\right)\sin\left[\frac{\omega_n z}{\sqrt{D_2}}\right]\right)^2 dz \right)}, \qquad [16e]$$

where Ξ is the determinant of the matrix in Eq. [11a], and Ξ_i is this determinant with the ith column replaced by the column of constants on the right-hand side of Eq. [11a]. Specifically,

$$\frac{\Xi_1}{\Xi} = \frac{\begin{bmatrix} 0 & 0 & \cdots \\ \sqrt{D_1}\cos\left[\frac{\omega_n a}{\sqrt{D_2}2}\right] & -\sqrt{D_2}\cos\left[\frac{\omega_n a}{\sqrt{D_2}2}\right] & \\ 0 & \sqrt{D_2}\cos\left[\frac{\omega_n(a/2+b)}{\sqrt{D_2}}\right] & \\ 0 & & \\ 0 & \left(\cos\left[\frac{\omega_n(a/2+b)}{\sqrt{D_2}2}\right]\omega_n\sqrt{D_2} + M\sin\left[\frac{\omega_n(a/2+b)}{\sqrt{D_2}2}\right]\right) & \\ 0 & 0 & \end{bmatrix}}{\Xi}$$

$$\frac{\begin{bmatrix} 0 & 0 & \cdots \\ 0 & 0 & \\ \sqrt{D_1}\sin\left[\frac{\omega_n(a/2+b)}{\sqrt{D_1}}\right] & -\sqrt{D_1}\cos\left[\frac{\omega_n(a/2+b)}{\sqrt{D_1}}\right] & \\ -\sqrt{D_1}\sin\left[\frac{\omega_n(3a/2+b)}{\sqrt{D_1}}\right] & \sqrt{D_1}\cos\left[\frac{\omega_n(3a/2+b)}{\sqrt{D_1}}\right] & \\ -M\cos\left[\frac{\omega_n(a/2+b)}{\sqrt{D_1}2}\right] & -M\sin\left[\frac{\omega_n(a/2+b)}{\sqrt{D_1}2}\right] & \\ \left(-\sin\left[\frac{\omega_n(3a/2+b)}{\sqrt{D_1}}\right]\omega_n\sqrt{D_1} + M\cos\left[\frac{\omega_n(3a/2+b)}{\sqrt{D_1}}\right]\right) & \left(\cos\left[\frac{\omega_n(3a/2+b)}{\sqrt{D_1}}\right]\omega_n\sqrt{D_1} + M\sin\left[\frac{\omega_n(3a/2+b)}{\sqrt{D_1}}\right]\right) & \end{bmatrix}}{\Xi}$$

$$\frac{\begin{bmatrix} -\sin\left[\frac{\omega_n 3(a+b)}{\sqrt{D_2}2}\right] & \cos\left[\frac{\omega_n 3(a+b)}{\sqrt{D_2}2}\right] \\ 0 & 0 \\ 0 & 0 \\ \sqrt{D_2}\sin\left[\frac{\omega_n(3a/2+b)}{\sqrt{D_2}}\right] & -\sqrt{D_2}\cos\left[\frac{\omega_n(3a/2+b)}{\sqrt{D_2}}\right] \\ 0 & 0 \\ -M\cos\left[\frac{\omega_n(3a/2+b)}{\sqrt{D_2}}\right] & -M\sin\left[\frac{\omega_n(3a/2+b)}{\sqrt{D_2}}\right] \end{bmatrix}}{\Xi} \quad [16f]$$

and

$$D_{1,n} = \frac{\left(\begin{array}{l} G_1 \sin\left[\frac{\zeta_n z_0}{\sqrt{D_1}}\right] + G_2\left\{\left(\frac{\Psi_1}{\Psi}\right)\cos\left[\frac{\zeta_n z_0}{\sqrt{D_2}}\right] + \left(\frac{\Psi_2}{\Psi}\right)\sin\left[\frac{\zeta_n z_0}{\sqrt{D_2}}\right]\right\} \\ \quad + G_3\left\{\left(\frac{\Psi_3}{\Psi}\right)\cos\left[\frac{\zeta_n z_0}{\sqrt{D_1}}\right] + \left(\frac{\Psi_4}{\Psi}\right)\sin\left[\frac{\zeta_n z_0}{\sqrt{D_1}}\right]\right\} + G_4\left\{\left(\frac{\Psi_5}{\Psi}\right)\cos\left[\frac{\zeta_n z_0}{\sqrt{D_2}}\right] + \left(\frac{\Psi_6}{\Psi}\right)\sin\left[\frac{\zeta_n z_0}{\sqrt{D_2}}\right]\right\} \end{array}\right)}{\left(\begin{array}{l} \int_0^{a/2}\left(\sin\left[\frac{\zeta_n z}{\sqrt{D_1}}\right]\right)^2 dz + \int_{a/2}^{a/2+b}\left(\left(\frac{\Psi_1}{\Psi}\right)\cos\left[\frac{\zeta_n z}{\sqrt{D_2}}\right] + \left(\frac{\Psi_2}{\Psi}\right)\sin\left[\frac{\zeta_n z}{\sqrt{D_2}}\right]\right)^2 dz \\ \quad + \int_{a/2+b}^{3a/2+b}\left(\left(\frac{\Psi_3}{\Psi}\right)\cos\left[\frac{\zeta_n z}{\sqrt{D_1}}\right] + \left(\frac{\Psi_4}{\Psi}\right)\sin\left[\frac{\zeta_n z}{\sqrt{D_1}}\right]\right)^2 dz + \int_{3a/2+b}^{a/3(a+b)/2}\left(\left(\frac{\Psi_5}{\Psi}\right)\cos\left[\frac{\zeta_n z}{\sqrt{D_2}}\right] + \left(\frac{\Psi_6}{\Psi}\right)\sin\left[\frac{\zeta_n z}{\sqrt{D_2}}\right]\right)^2 dz \end{array}\right)}, \quad [16g]$$

where Ψ is the determinant of the matrix in Eq. [11b] and Ψ_i is the determinant with the ith column replaced by the column of constants, as in Eq. [16f] above.

The Spin-echo signal. The expression for the PFGSE signal intensity, $E[q, \Delta]$, is obtained by substituting the expressions for P and Q into Eq. [1]. Thus,

$$E[q, \Delta] = \frac{2}{3(a+b)}\int_0^{3(a+b)/2}\int_0^{3(a+b)/2}\left(\sum_{j=1}^{4} G_j(P_j + Q_j)\right)\exp[i2\pi q(z - z_0)]dzdz_0. \quad [17a]$$

The Heaviside step-functions (Eqs. [13b] and [13c]) associated with P_1 and Q_1 restrict the domain of integration to [0, $a/2$], and for P_2 and Q_2 to [$a/2$, $(a + b)/2$], etc., for P_3 and Q_3, and P_4 and Q_4. Then Eq. [17a] is evaluated by using the real part of the Euler identity for the exponential part of the expression, i.e., $\cos[2\pi q(z - z_0)]$. Thus, we define

$$E[q, \Delta] = E_1[q, \Delta] + E_2[q, \Delta] + E_3[q, \Delta] \quad [17b]$$

and

$$\begin{aligned} E_1[q, \Delta] = \frac{2}{3(a+b)}\frac{1}{\Phi}\Bigg\{ & \int_0^{a/2}\cos\left[\frac{\omega_n z_0}{\sqrt{D_1}}\right]\int_0^{a/2}\cos\left[\frac{\omega_n z}{\sqrt{D_1}}\right]\exp[-\omega_n^2\Delta]\cos[2\pi q(z - z_0)]dzdz_0 \\ & + \int_0^{a/2}\cos\left[\frac{\omega_n z_0}{\sqrt{D_1}}\right]\int_{a/2}^{a/2+b}\left(\frac{\Xi_1}{\Xi}\cos\left[\frac{\omega_n z}{\sqrt{D_1}}\right] + \frac{\Xi_2}{\Xi}\sin\left[\frac{\omega_n z}{\sqrt{D_1}}\right]\right)\exp[-\omega_n^2\Delta]\cos[2\pi q(z - z_0)]dzdz_0 \\ & + \int_0^{a/2}\cos\left[\frac{\omega_n z_0}{\sqrt{D_1}}\right]\int_{a/2+b}^{3a/2+b}\left(\frac{\Xi_3}{\Xi}\cos\left[\frac{\omega_n z}{\sqrt{D_1}}\right] + \frac{\Xi_4}{\Xi}\sin\left[\frac{\omega_n z}{\sqrt{D_1}}\right]\right)\exp[-\omega_n^2\Delta]\cos[2\pi q(z - z_0)]dzdz_0 \\ & + \int_0^{a/2}\cos\left[\frac{\omega_n z_0}{\sqrt{D_1}}\right]\int_{3a/2+b}^{3(a+b)/2}\left(\frac{\Xi_5}{\Xi}\cos\left[\frac{\omega_n z}{\sqrt{D_1}}\right] + \frac{\Xi_6}{\Xi}\sin\left[\frac{\omega_n z}{\sqrt{D_1}}\right]\right)\exp[-\omega_n^2\Delta]\cos[2\pi q(z - z_0)]dzdz_0 \\ & + \int_{a/2}^{a/2+b}\left(\frac{\Xi_1}{\Xi}\cos\left[\frac{\omega_n z_0}{\sqrt{D_1}}\right] + \frac{\Xi_2}{\Xi}\sin\left[\frac{\omega_n z_0}{\sqrt{D_1}}\right]\right)\int_0^{a/2}\cos\left[\frac{\omega_n z}{\sqrt{D_1}}\right]\exp[-\omega_n^2\Delta]\cos[2\pi q(z - z_0)]dzdz_0 \\ & + \int_{a/2}^{a/2+b}\left(\frac{\Xi_1}{\Xi}\cos\left[\frac{\omega_n z_0}{\sqrt{D_1}}\right] + \frac{\Xi_2}{\Xi}\sin\left[\frac{\omega_n z_0}{\sqrt{D_1}}\right]\right)\int_{a/2}^{a/2+b}\left(\frac{\Xi_1}{\Xi}\cos\left[\frac{\omega_n z}{\sqrt{D_1}}\right] + \frac{\Xi_2}{\Xi}\sin\left[\frac{\omega_n z}{\sqrt{D_1}}\right]\right) \\ & \times \exp[-\omega_n^2\Delta]\cos[2\pi q(z - z_0)]dzdz_0 \\ & + \cdots 10 \text{ more terms consisting of combinations of integrals over the four domains of} z \text{ used previously}\Bigg\}, \end{aligned} \quad [17c]$$

where Φ is the denominator of Eq. [16e]. A similar expression exists for $E_2[q, \Delta]$ based on Q.

The final subexpression, $E_3[q, \Delta]$, which is readily obtained, arises because the root $\omega_n = 0$ is "allowed." Thus the additional term is

$$E_3[q, \Delta] = \frac{2}{3(a+b)} \int_0^{3(a+b)/2} \int_0^{3(a+b)/2} \cos[2\pi q(z - z_0)] dz dz_0 = \left(\frac{\sin\left[\pi q \frac{3(a+b)}{2} \right]}{\pi q \frac{3(a+b)}{2}} \right)^2 . \quad [17d]$$

The final, overall expression, $E_1[q, \Delta] + E_2[q, \Delta] + E_3[q, \Delta]$, derived from Eqs. [17a]–[17d], was obtained by using *Mathematica* (*23*). Because of its complicated nature it is not reproduced here; however, it was evaluated in a program written in *Mathematica* to yield simulations of experimental systems with various values of a, b, D_1, D_2, and M (see Results and Discussion).

METHODS

Computational methods. The *derivations* of many of the formulae used in the analysis, and the final program used to evaluate the expression for $E[q, \Delta]$ (Eq. [17]), were written in *Mathematica* (*24*).

The *random walk* simulations employed the basic procedures that have been described previously (*16*). However, the program was rewritten in Matlab (*30*) and the random-number generator was that provided by the "rand" function.

The *neural network* was selected from one in the "Neural Network Toolbox" (*30*) in Matlab (*31*); it was a back-propagation algorithm using the Levenberg–Marquardt minimization procedure. The neural network entailed 50 input elements and was trained with a set of 10 input vectors that were obtained from the *Mathematica* simulations, using 50 different q-values, selected values of a, b, D_1, and D_2, and 10 different values of M. Thus by a process of trial and error, guided by a compromise between the rate of convergence of the "training" process and the quality of the "fit" to "test" input data, the number of hidden neurodes was set to 6. The maximum number of "epochs" used for training was 300, and the "target" tolerance was set to 1.0×10^{-9}.

RESULTS

Evaluation of Eq. [17]. The solution of the problem expressed by Eq. [17] was programmed in *Mathematica* (*24*). The slowest part of the evaluation was the systematic finding of the roots of the transcendental equations (i.e., evaluating the determinants in Eqs. [9] and [10]). The infinite-polynomial series converged rapidly with the "physically realistic" parameters used for the various figures shown herein; routinely only four or six terms ($n = 4$ or 6 in Eq. [17]) were used to obtain the solutions. The relative contributions of the P and Q solutions to the overall result were also of interest; in general the final solution was dominated by that of P.

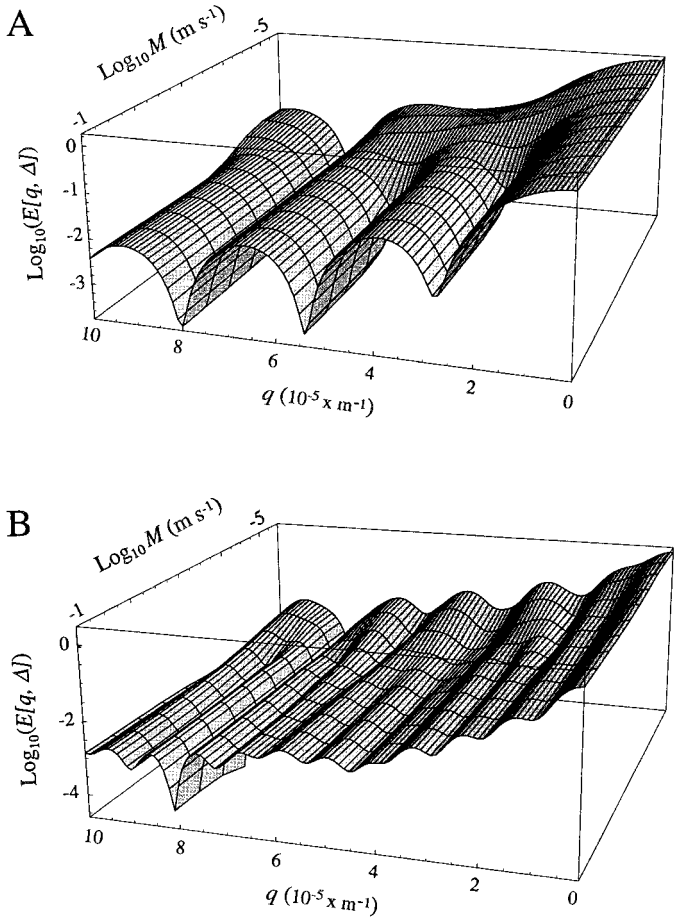

FIG. 2. Family of q-space plots, generated using the analytical theory (Eq. [17]), showing the dependence of their form on variations of the membrane permeability, M. The separation between the membranes in Region(s) 1 was set to $a = 5$ μm and that for Region(s) 2 was $b = 2.5$ μm; the values of the diffusion coefficients were $D_1 = D_2 = 1.0 \times 10^{-9}$ m^2 s^{-1}; and $\Delta = 10$ ms. (A) Solutions for the periodic two-region system as depicted in Fig. 1B. (B) Solutions for the four-region periodic system as depicted in Fig. 1C.

Dependence of the form of q-space plots on membrane permeability, M; a/b ratio a small integer. Figure 2A shows a series of q-space plots, graphed as a 3-dimensional surface, for spins diffusing in a system of parallel planes with separations that alternated between 5.0 and 2.5 μm. The permeability values used to generate the figures encompassed those observed experimentally for water ($\sim 10^{-4}$ m s^{-1}; *32*), monovalent anions such as chloride, bicarbonate, and fluoride ($\sim 2 \times 10^{-7}$ m s^{-1}; *33*), glucose ($\sim 4 \times 10^{-7}$ m s^{-1}; *34*), and ammonia ($\sim 2 \times 10^{-3}$ m s^{-1}; *35*). The diffusion coefficients were assigned a value similar to that of water, and low-molecular-

weight solutes at 37°C (*16*), and they were made equal to 1×10^{-9} m^2 s^{-1}.

Figure 2B shows q-space plots for the same scheme of parallel planes as above (Fig. 2A) but with the analysis carried out for a system with a periodicity of four regions. When the permeability is very large the membranes are effectively "transparent" to the diffusing spins, so it was not surprising that the coherence-pattern conformed to that expected for a periodicity (relative location of the minima in the plots) that was consistent with $2/(a + b) = 2/(7.5\ \mu\text{m}) = 266{,}000\ \text{m}^{-1}$ (for Fig. 2A) and $3/[2(a + b)] = 3/(2 \times 7.5\ \mu\text{m}) = 88{,}000\ \text{m}^{-1}$ (for Fig. 2B); the latter appear as small "ripples" on the plot. On the other hand, when the membrane permeability was very low, the coherence pattern corresponded to that of a system with an effective half-separation of the membranes of $a/2$ and $b/2$. The latter two distances for Figs. 2A and 2B differed by a factor of 2 so a very regular overall coherence pattern was apparent when there was superposition of the diffraction patterns for 1.25 and 2.5 μm. Hence the minima from *both* compartments would be expected to coincide at $q = 1/(1.25\ \mu\text{m}) = 800{,}000\ \text{m}^{-1}$, and this is evident in both Figs. 2A and 2B.

Dependence of the forms of q-space plots on permeability, M; ratio a/b a noninteger. For Figs. 3A and 3B, the separation between the parallel membranes was set to $a = 5\ \mu$m and $b = 4.8\ \mu$m. The coherence pattern for the situation in which there was a very high permeability gave a pattern that corresponded to $(a + b)/2 = 4.9\ \mu$m and $3(a + b)/2 = 9.8\ \mu$m for the two figures, respectively. On the other hand, when the permeability was low the superimposition of the two coherence patterns led to a much more complex pattern than for the counterparts in Fig. 2. This is because of the lack of a small integer relationship between the two spacings, namely 24:25 instead of 2:1 for Figs. 2 and 3, respectively.

Figure 4 was generated to provide a further impression of the dependence of the shape of the q-space plots on variations in the relative values of the diffusion coefficients in the compartments on either side of the membrane. The basic models were those used for Fig. 3 but with M fixed at 1.0×10^{-6} m s^{-1}. It was apparent that only when the value of the diffusion coefficient was such that it was not much greater than $b^2/2D_2$ did the pattern show any significant dependence on the value of D_2. Both the two- and the four-region solutions clearly showed a "major" minimum at $q = 800{,}000\ \text{m}^{-1}$.

Effect of Δ on the form of q-space plots. Figure 5 shows that changing Δ to a larger value, relative to that used for Fig. 3, smooths the q-space plots; it also changes the M-position at which the corrie (start of the 'glacial' valley) appears in the 3-dimensional plot. Thus the range of M values for which the experiment is sensitive is shifted to a lower mean.

Analysis of simulated data. The model used to generate Fig. 2A was used to provide data to train an artificial neural network (ANN; see Methods). Because it was clear that the form of the q-space plots in Fig. 2A were largely independent

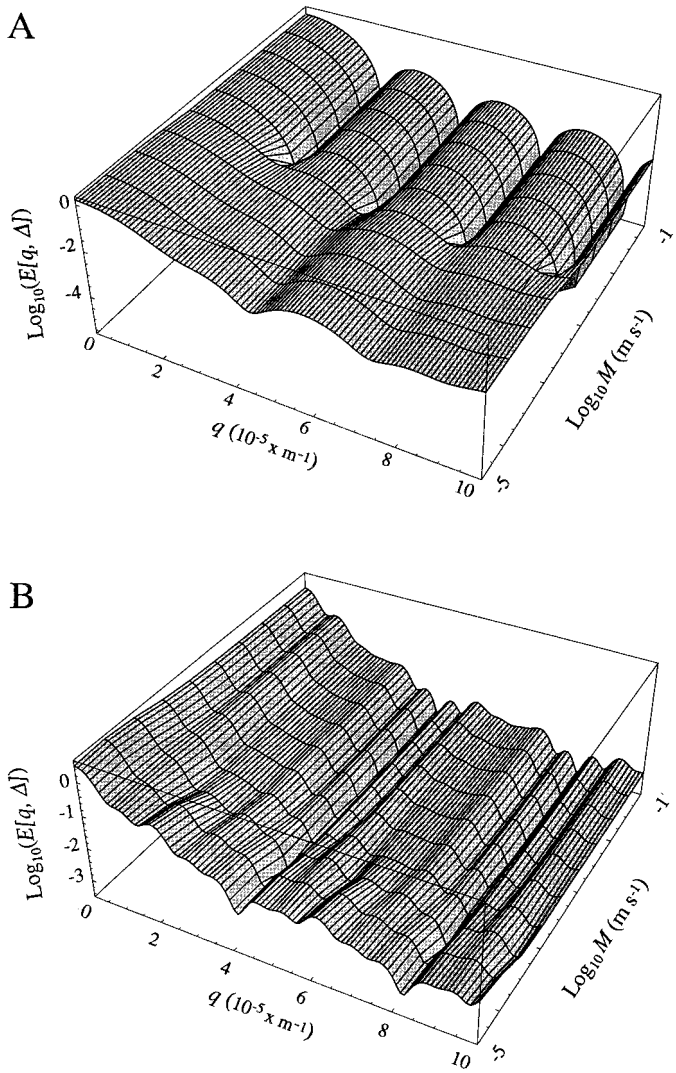

FIG. 3. Family of q-space plots for a range of membrane permeabilities but with membrane separations that were different from those used in Fig. 2. All parameters used in the simulation were the same as for Fig. 2 except $b = 4.8\ \mu$m, and the graphical-output "viewpoints" were changed to give a clearer impression of the plots with low M values. (A) Two-region system. (B) Four-region system.

of the value of M for the larger values used to generate it, a new set of data was generated for which M lay in the domain 2.0×10^{-4} to 2.0×10^{-3} m s^{-1}. The simulated data had 50 different q-values, hence the ANN had 50 input neurodes, and it had a hidden layer of 6 fully interconnected neurodes that had sigmoidal transfer functions; and the single output neurode had a linear transfer function. The input-vectors for the ANN were the natural logarithms of the relative PFGSE NMR signal intensities versus q, and the ANN was trained to yield the value of the permeability that had been used to generate each original data vector. The ability of the trained ANN to yield correct estimates of the permeability coefficient for each simulated experiment was tested by applying to it the

results of a simulated experiment for which the value of the permeability coefficient lay close to but was not one of these values (it, of course, lay within the overall range of those used for generating Figs. 2A and 2B). An example of one training "run" which took ~5 min to complete shows the actual value of M ($10^4 \times$ m s^{-1}) used to generate the original training vectors (data set) and the value returned by the trained ANN when it was "fed" the original data, respectively: 2.0, 2.0; 2.95, 2.95; 3.89, 3.89; 4.84, 4.8036; 5.79, 6.1855; 6.75, 6.6116; 7.68, 7.428; 8.63, 8.6885; 9.58, 9.2393; 14.32, 13.681. In addition, for example, when data from a simulation for which the value of M lay between those of the last two above (viz., 10.53×10^{-4} m s^{-1}) the "returned" value was 9.7134×10^{-4} m s^{-1}.

Monte Carlo simulations of diffusion between permeable parallel planes. Matlab was used to program the random-walk simulation of a system involving molecular diffusion in a region enclosed by a pair of parallel planes. It was assumed that the diffusion trajectory began in the region between the planes but that it could proceed beyond them by permeating the membranes according to a previously specified transition probability. Alternatively, the system could be treated as a purely two-region one with no exchange across the "outer" walls. Figure 6 (dots) shows the q-space plots predicted for the latter system consisting of 1×10^6 different trajectories. When periodic boundary conditions were applied the result, for the particular set of (biochemically realistic) values used, showed very little difference (data not shown). In other words, the two-region approximation is a "good" one for systems similar to water and low-molecular-weight solutes diffusing in and around cells in tissues or erythrocytes in a suspension.

Figure 6 also contains data that served to validate the analytical solution shown by the solid line (Eq. [17]). There was a close similarity for solutions obtained by both methods, but the evaluation of the analytical solution was achieved ~100 times faster.

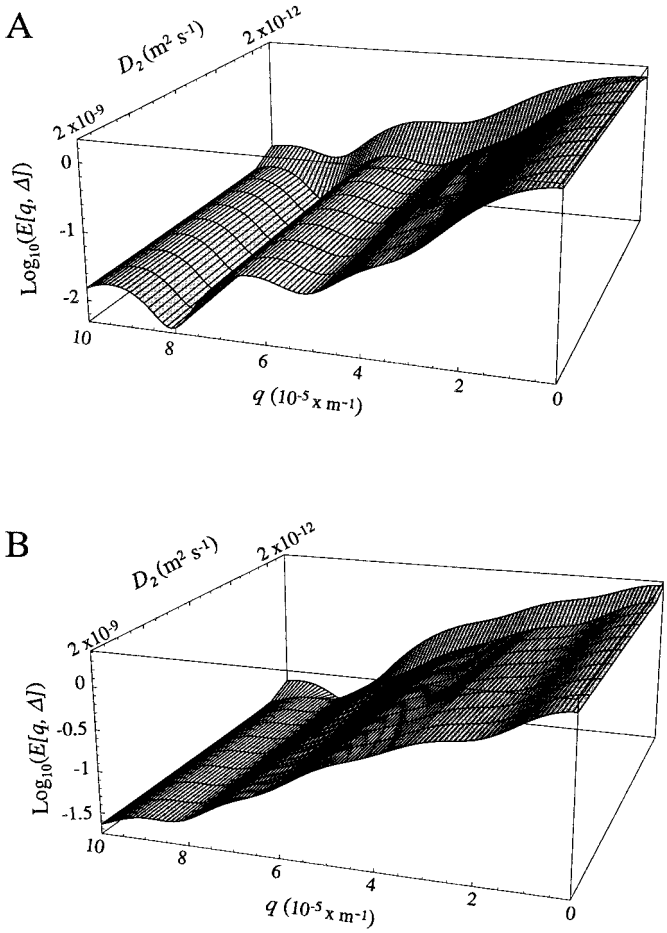

FIG. 4. Evaluations of the analytical solution for the periodic two-region system showing the dependence of the form of the plots on the value of the diffusion coefficient, D_2, of the spins in the second region. The value of M was 1.0×10^{-6} m s^{-1}, and the other parameters were as for Fig. 2A. (A) Two-region periodicity and (B) four-region periodicity.

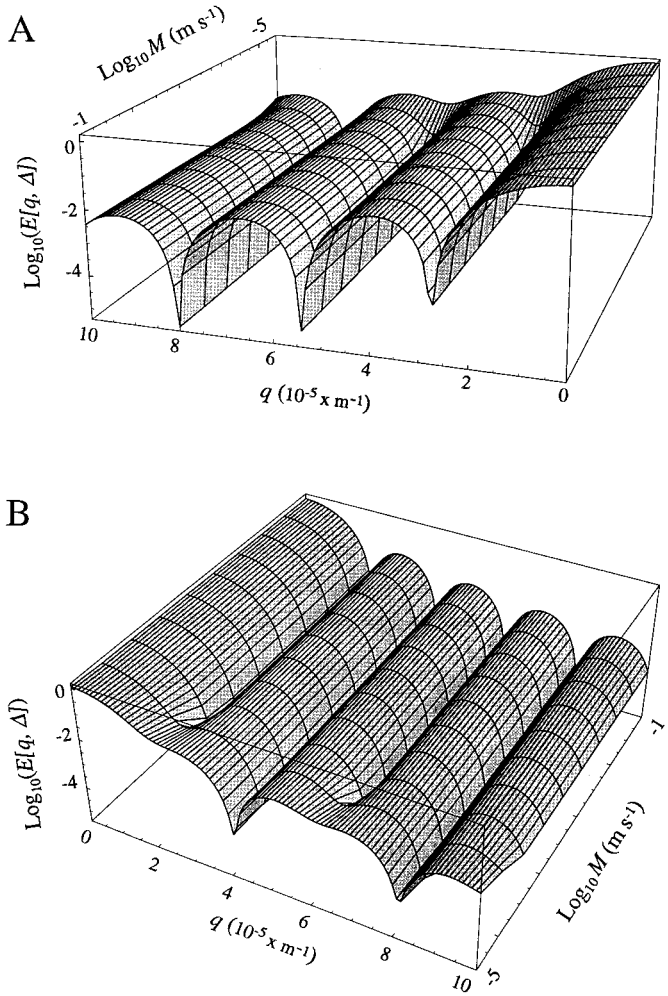

FIG. 5. The effect of increasing Δ from 10 ms (in Fig. 3) to 100 ms on the q-space plots. All other parameters used in the evaluations were the same as for the respective panels in Fig. 3. (A) Two-region periodicity and (B) four-region periodicity. Note that different "viewpoints" were used for each panel.

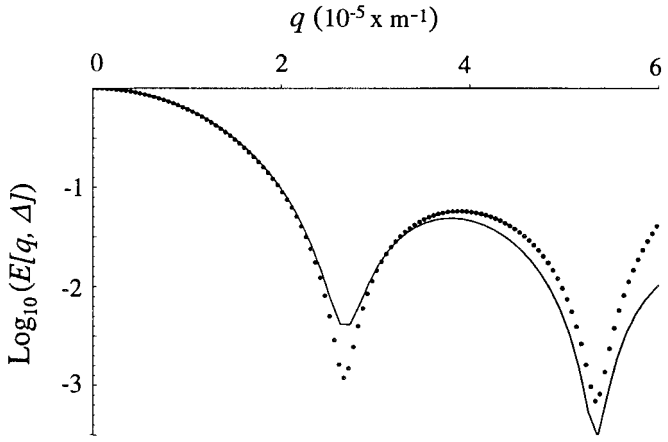

FIG. 6. Comparison of the analytical solution (Eq. [17]; solid line) for a two-region periodicity (data from Fig 2A) and a random-walk simulation (dots) for two compartments with a separating membrane. For this particular pair of evaluations/simulations the permeability of the membranes was made high ($M = 0.1$ m s^{-1} for the analytical solution, and a transition probability of 0.9999 was used for the Monte Carlo simulation).

DISCUSSION

Dependence of the forms of q-space plots on membrane permeability; ratio a/b a small integer. The first minima evident in the coherence patterns of Fig. 2, when the diffusing spins were confined to move only between, and not through, the membranes, were at $2/a$ and $2/b$. This outcome is consistent with the simulated results presented by Callaghan (*9*), taking special note of the way the boundary conditions were set up here. For the simulations in which the membranes were specified as being very permeable the effective spacing between the barriers became $(a + b)/2$ for the simulated two-region system and $3(a + b)/2$ for the four-region system. This is the result anticipated from the earlier work (*9*) and it emphasizes the analogy between the present coherence phenomena and that of single-slit diffraction in physical optics (*36*).

Dependence of the forms of q-space plots on permeability; a/b ratio a noninteger. It is evident that for a real system in which there is not a simple integer relationship between the spacings of the parallel membranes that the periodic structure of the q-space plot can be quite complicated. Variations in a, b, and M, therefore, can generate q-space plots whose form may, possibly, not be able to be analyzed to yield unique estimates of the three parameters because of this lack of "graphical features."

ANN analysis. An ANN was able to be rapidly trained with synthetic data obtained by evaluating the analytical expression in Eq. [17], and the ANN was then used to analyze data not used in the training set. In principle real experimental data could be analyzed this way provided the model was a realistic representation of the experimental system. Also, the estimates of errors from such a fitting exercise would require repeated training of the ANN and appropriate statistical analysis of the outputs (e.g., Ref. *37*).

The procedure to demonstrate the proposed data analysis (fitting) that uses an ANN was applied to estimate only one parameter. The much more difficult task of fitting two or more parameters is potentially complicated by nonuniqueness of the fits and only weak dependence of the various features of the q-space plots on particular parameter values. This area of analysis of "real/experimental" q-space plots requires further development.

Monte Carlo simulations of diffusion between permeable parallel planes. The time taken to generate the q-space plots using a random-walk simulation of diffusion was significantly greater than for evaluations of the analytical solutions; the time difference was ~100-fold (depending on the number of trajectories used in the random-walk analysis). This outcome implies that although the analytical solution (Eq. [17]) is very complicated, the time taken for its evaluation is substantially less than that required to perform a Monte Carlo random-walk simulation of the corresponding system. Hence, to provide data for the purposes of training an ANN, the analytical solution is superior. However, if the real system is not well described by the analytical system then it will be necessary to resort to the Monte Carlo procedure (*37, 38*).

Conclusions. The analytical solutions that have been presented here enable the simulation of q-space plots for systems that are "realistic" but admittedly only relatively loose models of a suspension of cells or a tissue. Nevertheless, evaluation of the solutions provides insights into the effects of changes in membrane spatial arrangement and permeability on the form of q-space plots, in a manner that appears not to have been presented before.

ACKNOWLEDGMENTS

The work was funded by a grant from the Australian Research Council. Drs. Bob Chapman, Allan Torres, and Bill Bubb and Mr. David Regan are thanked for valuable discussions. Mr. Bill Lowe is thanked for expert technical and computing assistance.

REFERENCES

1. D. G. Cory and A. N. Garroway, *Magn. Reson. Med.* **14,** 435 (1990).
2. P. T. Callaghan, A. Coy, D. MacGowan, K. J. Packer, and F. O. Zelaya, *Nature* **351,** 467 (1991).
3. P. T. Callaghan, A. Coy, T. P. J. Halpin, D. MacGowan, K. J. Packer, and F. O. Zelaya, *J. Chem. Phys.* **97,** 651 (1991).
4. P. P. Mitra and P. N. Sen, *Phys. Rev. B* **45,** 143 (1992).
5. P. T. Callaghan, "Principles of Magnetic Resonance Microscopy," Oxford Univ. Press, Oxford (1991).
6. P. W. Kuchel, A. Coy, and P. Stilbs, *Magn. Reson. Med.* **37,** 637 (1997).
7. M. King, J. Housman, D. G. Gadian, and A. Connelly, *Magn. Reson. Med.* **38,** 930 (1997).
8. P. T. Callaghan, and A. Coy, *in* "Nuclear Magnetic Resonance Probes of Molecular Dynamics" (R. Tycko, Ed.), Kluwer, Amsterdam (1994).

9. P. T. Callaghan, *J. Magn. Reson. A* **113,** 53 (1995).

10. A. V. Barzykin, K. Hayamizu, W. S. Price, and M. Tachiya, *J. Magn. Reson. A* **114,** 39 (1995).

11. W. S. Price, A. V. Barzykin, K. Hayamizu, and M. Tachiya, *Biophys. J.* **74,** 2259 (1998).

12. A. M. Torres, R. J. Michniewicz, B. E. Chapman, G. A. R. Young, and P. W. Kuchel, *Magn. Reson. Imaging* **16,** 423 (1998).

13. M. Appel, G. Fleischer, D. Geschke, J. Karger, and M. Winkler, *J. Magn. Reson. A* **122,** 248 (1996).

14. J. E. Tanner, *J. Chem. Phys.* **69,** 1748 (1978).

15. J. E. M. Snaar and H. Van As, *J. Magn. Reson. A* **102,** 318 (1993).

16. A. J. Lennon and P. W. Kuchel, *J. Magn. Reson. A* **107,** 229 (1994).

17. A. J. Lennon, "A Pulsed Field Gradient NMR and Random-Walk Simulation Study of Diffusion in Heterogeneous Systems," Ph.D. dissertation, Department of Biochemistry, University of Sydney (1995).

18. J. Karger and W. Heink, *J. Magn. Reson.* **51,** 1 (1983).

19. P. W. Kuchel, A. J. Lennon, and C. Durrant, *J. Magn. Reson. B* **112,** 1 (1996).

20. B. Balinov, B. Jonsson, P. Linse, and O. Soderman, *J. Magn. Reson. A* **104,** 17 (1993).

21. O. Soderman and B. Jonsson, *J. Magn. Reson. A* **117,** 94 (1995).

22. A. R. Waldeck, P. W. Kuchel, A. J. Lennon, and B. E. Chapman, *Prog. NMR Spectrosc.* **30,** 39 (1997).

23. G. P. Mulholland and M. H. Cobble, *Int. J. Heat Mass Transfer* **15,** 147 (1972).

24. S. Wolfram, "The Mathematica Book," (3rd ed.) Cambridge Univ. Press, Cambridge (1996).

25. I. N. Sneddon, "Special Functions of Mathematical Physics and Chemistry," Oliver & Boyd, Edinburgh (1956).

26. P. Moon and D. Spencer, "Field Theory for Engineers," Van Nostrand, Princeton, NJ (1961).

27. P. Moon and D. Spencer, "Field Theory Handbook," 2nd ed., Springer-Verlag, Berlin (1988).

28. J. S. Murday and R. M. Cotts, *J. Chem. Phys.* **48,** 4938 (1968).

29. C. H. Neuman, *J. Chem. Phys.* **60,** 4508 (1974).

30. D. Handelsman and B. Littlefield, "Mastering Matlab," Prentice-Hall, Upper Saddle River, NJ (1995).

31. H. Demuth and M. Beale, "Neural Network Toolbox," (version 3), The Maths Works Inc., Natick, MA (1998).

32. Gh. Benga, V. I. Pop, O. Popescu, and V. Borza, *J. Biochem. Biophys. Methods* **21,** 87 (1990).

33. B. E. Chapman and P. W. Kuchel, *Eur. Biophys. J.* **19,** 41 (1990).

34. J. R. Potts and P. W. Kuchel, *Biochem. J.* **281,** 753 (1992).

35. R. J. Labotka, U. P. Lundberg, and P. W. Kuchel, *Am. J. Physiol.* **268,** C686 (1995).

36. F. A. Jenkins and H. E. White, "Fundamentals of Optics," 3rd ed., McGraw–Hill, New York, (1957).

37. A. J. Lennon and P. W. Kuchel, *Proc. IEEE Intl. Conf. Neural Networks, Perth WA,* 2473 (1995).

38. A. M. Torres, A. T. Taurins, D. G. Regan, B. E. Chapman, and P. W. Kuchel, *J. Magn. Reson.* **138,** 135 (1999).